NASA/TM—2017-219492

Incorporation of Failure Into an Orthotropic Three-Dimensional Model With Tabulated Input Suitable for Use in Composite Impact Problems

Robert K. Goldberg
Glenn Research Center, Cleveland, Ohio

Kelly S. Carney and Paul DuBois
George Mason University, Fairfax, Virginia

Canio Hoffarth, Bilal Khaled, Loukham Shyamsunder, and Subramaniam Rajan
Arizona State University, Tempe, Arizona

Gunther Blankenhorn
Livermore Software Technology Corporation, Livermore, California

May 2017

NASA STI Program . . . in Profile

Since its founding, NASA has been dedicated to the advancement of aeronautics and space science. The NASA Scientific and Technical Information (STI) Program plays a key part in helping NASA maintain this important role.

The NASA STI Program operates under the auspices of the Agency Chief Information Officer. It collects, organizes, provides for archiving, and disseminates NASA's STI. The NASA STI Program provides access to the NASA Technical Report Server—Registered (NTRS Reg) and NASA Technical Report Server—Public (NTRS) thus providing one of the largest collections of aeronautical and space science STI in the world. Results are published in both non-NASA channels and by NASA in the NASA STI Report Series, which includes the following report types:

- TECHNICAL PUBLICATION. Reports of completed research or a major significant phase of research that present the results of NASA programs and include extensive data or theoretical analysis. Includes compilations of significant scientific and technical data and information deemed to be of continuing reference value. NASA counter-part of peer-reviewed formal professional papers, but has less stringent limitations on manuscript length and extent of graphic presentations.

- TECHNICAL MEMORANDUM. Scientific and technical findings that are preliminary or of specialized interest, e.g., "quick-release" reports, working papers, and bibliographies that contain minimal annotation. Does not contain extensive analysis.

- CONTRACTOR REPORT. Scientific and technical findings by NASA-sponsored contractors and grantees.

- CONFERENCE PUBLICATION. Collected papers from scientific and technical conferences, symposia, seminars, or other meetings sponsored or co-sponsored by NASA.

- SPECIAL PUBLICATION. Scientific, technical, or historical information from NASA programs, projects, and missions, often concerned with subjects having substantial public interest.

- TECHNICAL TRANSLATION. English-language translations of foreign scientific and technical material pertinent to NASA's mission.

For more information about the NASA STI program, see the following:

- Access the NASA STI program home page at http://www.sti.nasa.gov

- E-mail your question to help@sti.nasa.gov

- Fax your question to the NASA STI Information Desk at 757-864-6500

- Telephone the NASA STI Information Desk at 757-864-9658

- Write to:
  NASA STI Program
  Mail Stop 148
  NASA Langley Research Center
  Hampton, VA 23681-2199

NASA/TM—2017-219492

Incorporation of Failure Into an Orthotropic Three-Dimensional Model With Tabulated Input Suitable for Use in Composite Impact Problems

Robert K. Goldberg
Glenn Research Center, Cleveland, Ohio

Kelly S. Carney and Paul DuBois
George Mason University, Fairfax, Virginia

Canio Hoffarth, Bilal Khaled, Loukham Shyamsunder, and Subramaniam Rajan
Arizona State University, Tempe, Arizona

Gunther Blankenhorn
Livermore Software Technology Corporation, Livermore, California

National Aeronautics and
Space Administration

Glenn Research Center
Cleveland, Ohio 44135

May 2017

Acknowledgments

Authors Hoffarth, Khaled, Shyamsunder and Rajan gratefully acknowledge the support of (a) the Federal Aviation Administration through Grant #12-G-001 titled "Composite Material Model for Impact Analysis," William Emmerling, Technical Monitor, and (b) NASA through Contract Number: NN15CA32C titled "Development and Implementation of an Orthotropic Plasticity Progressive Damage Model for Transient Dynamic/Impact Finite Element Analysis of Composite Structures," Robert Goldberg, Contracting Officer Representative.

This work was sponsored by the Advanced Air Vehicle Program at the NASA Glenn Research Center

Level of Review: This material has been technically reviewed by technical management.

Available from

NASA STI Program
Mail Stop 148
NASA Langley Research Center
Hampton, VA 23681-2199

National Technical Information Service
5285 Port Royal Road
Springfield, VA 22161
703-605-6000

This report is available in electronic form at http://www.sti.nasa.gov/ and http://ntrs.nasa.gov/

Incorporation of Failure Into an Orthotropic Three-Dimensional Model With Tabulated Input Suitable for Use in Composite Impact Problems

Robert K. Goldberg
National Aeronautics and Space Administration
Glenn Research Center
Cleveland, Ohio 44135

Kelly S. Carney and Paul DuBois
George Mason University
Fairfax, Virginia 22030

Canio Hoffarth, Bilal Khaled, Loukham Shyamsunder, and Subramaniam Rajan
Arizona State University
Tempe, Arizona 85281

Gunther Blankenhorn
Livermore Software Technology Corporation
Livermore, California 94551

Abstract

The need for accurate material models to simulate the deformation, damage and failure of polymer matrix composites under impact conditions is becoming critical as these materials are gaining increased use in the aerospace and automotive communities. The aerospace community has identified several key capabilities which are currently lacking in the available material models in commercial transient dynamic finite element codes. To attempt to improve the predictive capability of composite impact simulations, a next generation material model is being developed for incorporation within the commercial transient dynamic finite element code LS-DYNA. The material model, which incorporates plasticity, damage and failure, utilizes experimentally based tabulated input to define the evolution of plasticity and damage and the initiation of failure as opposed to specifying discrete input parameters such as modulus and strength. The plasticity portion of the orthotropic, three-dimensional, macroscopic composite constitutive model is based on an extension of the Tsai-Wu composite failure model into a generalized yield function with a nonassociative flow rule. For the damage model, a strain equivalent formulation is used to allow for the uncoupling of the deformation and damage analyses. In the damage model, a semicoupled approach is employed where the overall damage in a particular coordinate direction is assumed to be a multiplicative combination of the damage in that direction resulting from the applied loads in various coordinate directions. For the failure model, a tabulated approach is utilized in which a stress or strain based invariant is defined as a function of the location of the current stress state in stress space to define the initiation of failure. Failure surfaces can be defined with any arbitrary shape, unlike traditional failure models where the mathematical functions used to define the failure surface impose a specific shape on the failure surface. In the current paper, the complete development of the failure model is described and the generation of a tabulated failure surface for a representative composite material is discussed.

Introduction

As composite materials are gaining increased use in aircraft components where impact resistance is critical (such as the turbine engine fan case), the need for accurate material models to simulate the deformation, damage and failure response of polymer matrix composites under impact conditions is

gaining in importance. While there are several material models currently available within commercial transient dynamic codes such as LS-DYNA (Ref. 1) to analyze the impact response of composites, areas have been identified where the predictive capabilities of these models can be improved. Most importantly, the existing models often require extensive correlation based on structural level impact tests, which significantly limits the ability to use these models as predictive tools. Furthermore, most of the existing models apply either a plasticity based approach (such as that used by Sun and Chen (Ref. 2)) or a continuum damage mechanics approach (such as that used by Matzenmiller et al. (Ref. 3)) to simulate the nonlinearity that takes place in the composite response. As documented in detail by Goldberg, et al. (Refs. 4 and 5), either of these approaches can capture certain aspects of the actual composite behavior. However, optimally, combining a plasticity based deformation model (to capture the rate dependence and significant nonlinearity, particularly in shear, observed in the composite response) with a damage model (to account for the changes in the unloading modulus observed as the material is unloaded from various stress levels, as well as to account for strain softening observed after the peak stress is reached) can provide advantages over using one approach or the other. In addition, the input to current material models generally consists of point-wise properties (such as the modulus, failure stress or failure strain in a particular coordinate direction) that leads to curve fit approximations to the material stress-strain curves. This type of approach either leads to models with only a few parameters, which provide a crude approximation at best to the actual material response, or to models with many parameters which require a large number of complex tests to characterize. An improved approach is to use tabulated data, obtained from a well-defined set of straightforward experiments. Using tabulated data allows the actual material response data to be entered in a discretized form, which permits a more accurate representation of the actual material response.

To begin to address these needs, a new composite material model is being developed and implemented for use within LS-DYNA. The material model is meant to be a fully generalized model suitable for use with any composite architecture (laminated or textile). The deformation model is based on extending the commonly used Tsai-Wu composite failure model (Ref. 6) to a strain hardening plasticity model with a nonassociative flow rule. For the damage model, a strain equivalent formulation is used in which the deformation and damage calculations can be uncoupled. A significant feature in the developed damage model is that a semicoupled approach has been utilized in which a load in a particular coordinate direction results in damage (and thus stiffness reduction) in multiple coordinate directions. While different from the approach used in many existing damage mechanics models (Ref. 3), in which a load in a particular coordinate direction only leads to a stiffness reduction in the load direction, this approach has the potential to more accurately reflect the damage behavior that actually takes place, particularly for composites with more complex fiber architectures.

A wide variety of failure models, which mark the end of the stress-strain curve, have been developed for composites. In models such as the Tsai-Wu failure model (Ref. 6), a quadratic function of the macroscopic stresses is defined in which the coefficients of the failure function are related to the tensile, compressive and shear failure stresses in the various coordinate directions. This model, while mathematically simple and easy to implement numerically, assumes that the composite failure surface has an ellipsoidal (in 2D) or ovoid (in 3D) shape. In reality, composite failure surfaces often are not in the form of simple shapes. More complex models, such as the Hashin model (Ref. 7), also utilize quadratic combinations of the macroscopic failure stresses, but utilize only selective terms in the quadratic function in order to link the macroscopic stresses to local failure modes such as fiber or matrix failure. However, an overall quadratic form to the failure functions (albeit in a piecewise fashion) are still assumed. This approach was extended in models such as those developed by Puck et al. (Ref. 8), Pinho et al. (Ref. 9) and Maimi et al. (Ref. 10), in which complex equations were developed to predict local failure mechanisms in terms of macroscopic level stresses. In this manner, the failure response and complex failure surfaces present in actual composites could be more accurately represented. However, in these advanced models, very complex tests are often required to characterize the model parameters and the applicability of the models may be limited to specific composite architectures with specific failure mechanisms. In a combination of approaches, researchers such as Mayes and Hansen (Ref. 11) and Feng (Ref. 12) utilize an

approach where stress (or strain) invariants based on macroscopic stresses are used to define the initiation of failure. However, different forms of the invariants are used to determine whether fiber-dominated or matrix-dominated failure occurs. Given the variety of failure models present in the literature, activities such as the World Wide Failure Exercise and its multiple iterations (e.g., Refs. 13 to 15) have attempted to conduct a rigorous review of which failure model or models provides the optimum prediction of composite failure. In all of these studies, none of the examined models showed a complete ability to predict composite failure or displayed a significant advantage compared to the other models examined.

The difficulty in simulating composite failure can be related to the fact that in reality failure is a highly localized phenomenon dependent on various combination of fiber, matrix and interface failures. Due to these complex and interacting local failure mechanisms, and the fact that these mechanisms can vary based on the constituent materials and fiber architecture, in reality the actual composite failure surface often does not conform to a shape that can be easily simulated using a simple mathematical function. Conversely, attempts to utilize discrete functions to analyze the complex local mechanisms can result in models with a large number of parameters that require a highly complex test program to obtain. In the methodology described in this paper, an approach is used in which the actual experimental three-dimensional failure envelope for a composite is entered in a tabulated fashion. Specifically, a stress or strain based invariant leading to the initiation of failure is defined as a function of the location of the current stress state in stress space. In this manner, an arbitrary failure surface can be easily defined based on actual experimental data in combination with numerical data obtained using any desired existing failure model. The current approach thus serves as a general framework which is not limited to any arbitrarily imposed failure surface based on an arbitrarily defined mathematical function.

In the following sections of this paper, a brief summary of the plasticity-based deformation model is presented. The key aspects of the damage model and its characterization are then described. Details of the failure model are then discussed, including the overall methodology along with its application for a representative composite material.

Deformation Model Overview

A complete description of the deformation model is given in Goldberg et al. (Refs. 4 and 5). A summary of the key features of the model is presented here. In the deformation model, a general quadratic three-dimensional orthotropic yield function based on the Tsai-Wu failure model is specified as follows, where 1, 2, and 3 refer to the principal material directions:

$$f(\sigma) = -1 + \begin{pmatrix} F_1 & F_2 & F_3 & 0 & 0 & 0 \end{pmatrix} \begin{pmatrix} \sigma_{11} \\ \sigma_{22} \\ \sigma_{33} \\ \sigma_{12} \\ \sigma_{23} \\ \sigma_{31} \end{pmatrix} + \begin{pmatrix} \sigma_{11} & \sigma_{22} & \sigma_{33} & \sigma_{12} & \sigma_{23} & \sigma_{31} \end{pmatrix} \begin{pmatrix} F_{11} & F_{12} & F_{13} & 0 & 0 & 0 \\ F_{12} & F_{22} & F_{23} & 0 & 0 & 0 \\ F_{13} & F_{23} & F_{33} & 0 & 0 & 0 \\ 0 & 0 & 0 & F_{44} & 0 & 0 \\ 0 & 0 & 0 & 0 & F_{55} & 0 \\ 0 & 0 & 0 & 0 & 0 & F_{66} \end{pmatrix} \begin{pmatrix} \sigma_{11} \\ \sigma_{22} \\ \sigma_{33} \\ \sigma_{12} \\ \sigma_{23} \\ \sigma_{31} \end{pmatrix} \tag{1}$$

In the yield function, σ_{ij} represents the stresses and F_{ij} and F_k are coefficients that evolve and are functions of the current values of the stresses in the various coordinate directions. By allowing the coefficients to vary, the yield surface evolution and hardening in each of the material directions can be

precisely defined. The values of the normal and shear coefficients can be determined by simplifying the yield function for the case of unidirectional tensile and compressive loading in each of the coordinate directions along with shear tests in each of the shear directions. In the above equation, the stresses are the current value of the yield stresses in the normal and shear directions. To determine the values of the off-axis coefficients (which are required to capture the stress interaction effects), the results from 45° off-axis tests (an arbitrarily chosen angle) in the various coordinate directions can be used. The values of the off-diagonal terms in the yield function can also be modified as required in order to ensure that the yield surface is convex (Ref. 5).

A nonassociative flow rule is used to compute the evolution of the components of plastic strain. The plastic potential for the flow rule is shown in Equation (2):

$$h = \sqrt{\begin{aligned} &H_{11}\sigma_{11}^2 + H_{22}\sigma_{22}^2 + H_{33}\sigma_{33}^2 + 2H_{12}\sigma_{11}\sigma_{22} + 2H_{23}\sigma_{22}\sigma_{33} + 2H_{31}\sigma_{33}\sigma_{11} \\ &\quad + H_{44}\sigma_{12}^2 + H_{55}\sigma_{23}^2 + H_{66}\sigma_{31}^2 \end{aligned}} \tag{2}$$

where σ_{ij} are the current values of the stresses and H_{ij} are independent coefficients, which are assumed to remain constant. The values of the coefficients are computed based on average plastic Poisson's ratios (Refs. 4 and 5). The plastic potential function in Equation (2) is used in a flow law to compute the components of the plastic strain rate, where the usual normality hypothesis from classical plasticity (Ref. 16) is assumed to apply and the variable $\dot{\lambda}$ is a scalar plastic multiplier:

$$\dot{\boldsymbol{\varepsilon}}^p = \dot{\lambda}\frac{\partial h}{\partial \boldsymbol{\sigma}} \tag{3}$$

Given the flow law, the principal of the equivalence of plastic work (Ref. 16) can be used to determine that the plastic potential function, h, can be defined as the effective stress and the plastic multiplier can be defined as the effective plastic strain rate.

To compute the current value of the yield stresses needed for the yield function, tabulated stress-strain curves are used to track the yield stress evolution. The user is required to input twelve stress versus plastic strain curves. Specifically, the required curves include uniaxial tension curves in each of the normal directions (1,2,3), uniaxial compression curves in each of the normal directions (1,2,3), shear stress-strain curves in each of the shear directions (1-2, 2-3, and 3-1), and 45° off-axis tension or compression curves in each of the 1-2, 2-3, and 3-1 planes. The 45° curves are required in order to properly capture the stress interaction effects. By utilizing tabulated stress-strain curves to track the evolution of the deformation response, the experimental stress-strain response of the material can be captured exactly without any curve fit approximations. The required stress-strain data can be obtained either from actual experimental test results or by appropriate numerical experiments utilizing stand-alone codes. The ability to account for rate and temperature effects has also been incorporated into the deformation model. To track the evolution of the deformation response along each of the stress-strain curves, the effective plastic strain is chosen to be the tracking parameter. Using a numerical procedure based on the radial return method (Ref. 16) in combination with an iterative approach, the effective plastic strain is computed for each time/load step. The stresses for each of the tabulated input curves corresponding to the current value of the effective plastic strain are then used to compute the yield function coefficients.

Damage Model Overview

The deformation portion of the material model provides the majority of the capability of the model to simulate the nonlinear stress-strain response of the composite. However, in order to capture the changes in the unloading modulus observed as the material is unloaded from various stress levels and the local softening of the stress-strain response that is often observed in composites (Ref. 17), a complementary

damage law is required. Strain equivalence is assumed in the damage law formulation, therefore the total, elastic and plastic strains in the actual and effective stress spaces are the same for every time step (Ref. 18). The utilization of strain equivalence permits the plasticity and damage calculations to be uncoupled, as all of the plasticity computations can take place in the effective stress space.

The first step in the development of the damage model is to relate the actual stresses to a set of effective stresses by use of a damage tensor **M**:

$$\boldsymbol{\sigma} = \mathbf{M}\boldsymbol{\sigma}_{eff} \tag{4}$$

The effective stress rate tensor can be related to the total and plastic strain rate tensors by use of the standard elasto-plastic constitutive equation

$$\dot{\boldsymbol{\sigma}}_{eff} = \mathbf{C}\left(\dot{\boldsymbol{\varepsilon}} - \dot{\boldsymbol{\varepsilon}}_{p}\right) \tag{5}$$

where **C** is the standard elastic stiffness matrix and the actual total and plastic strain rate tensors are used due to the strain equivalence assumption.

Given the usual assumption that the actual stress tensor and the effective stress tensor are symmetric, the actual stresses can be related to the effective stresses in the following manner, where the damage tensor **M** is assumed to have a maximum of 36 independent components:

$$\begin{pmatrix} \sigma_{11} \\ \sigma_{22} \\ \sigma_{33} \\ \sigma_{12} \\ \sigma_{23} \\ \sigma_{13} \end{pmatrix} = [\mathbf{M}] \begin{pmatrix} \sigma_{11}^{\text{eff}} \\ \sigma_{22}^{\text{eff}} \\ \sigma_{33}^{\text{eff}} \\ \sigma_{12}^{\text{eff}} \\ \sigma_{23}^{\text{eff}} \\ \sigma_{13}^{\text{eff}} \end{pmatrix} \tag{6}$$

In order to maintain a one to one relationship between the effective stresses and the actual stresses (i.e., to ensure that a uniaxial load in the actual stress space does not result in a multiaxial load in the effective stress space), the damage tensor is assumed to be diagonal, leading to the following form:

$$[\mathbf{M}] = \begin{bmatrix} M_{11} & 0 & 0 & 0 & 0 & 0 \\ 0 & M_{22} & 0 & 0 & 0 & 0 \\ 0 & 0 & M_{33} & 0 & 0 & 0 \\ 0 & 0 & 0 & M_{44} & 0 & 0 \\ 0 & 0 & 0 & 0 & M_{55} & 0 \\ 0 & 0 & 0 & 0 & 0 & M_{66} \end{bmatrix} \tag{7}$$

An implication of a diagonal damage tensor is that loading the composite in a particular coordinate direction only leads to a stiffness reduction in the direction of the load due to the formation of matrix cracks perpendicular to the direction of the load. However, as discussed in detail in Goldberg, et al. (Ref. 5), in actual composites, particularly those with complex fiber architectures, a load in one coordinate direction can lead to stiffness reductions in multiple coordinate directions. To maintain a diagonal damage tensor while still allowing for the damage interaction in at least a semicoupled sense, each term in the diagonal damage matrix should be a function of the plastic strains in each of the normal

and shear coordinate directions, for example the M_{11} term for the plane stress case has the strain dependences shown below:

$$M_{11} = M_{11}\left(\varepsilon_{11}^{p}, \varepsilon_{22}^{p}, \varepsilon_{12}^{p}\right) \tag{8}$$

Note that plastic strains are chosen as the "tracking parameter" due to the fact that, within the context of the developed formulation, the material nonlinearity during loading is simulated by use of a plasticity based model. The plastic strains therefore track the current state of load and deformation in the material. To explain this concept of damage coupling further, assume a load is applied in the 1-direction to an undamaged specimen. The undamaged modulus in the 1-direction is E_{11} and the undamaged modulus in the 2-direction is E_{22}. The stress-strain response of the material is assumed to become nonlinear (represented in the current model by the accumulation of plastic strain) and damage is assumed to occur. The original specimen is unloaded and reloaded elastically in the 1-direction. Due to the damage, the reloaded specimen has a reduced modulus in the 1-direction of E_{11}^{d11}. The reduced area and modulus are a function of the damage induced by the loading and resulting nonlinear deformation in the 1-direction (reflected as plastic strain) as follows:

$$E_{11}^{d11} = \left(1 - d_{11}^{11}\left(\varepsilon_{11}^{p}\right)\right)E_{11} \tag{9}$$

where d_{11}^{11} is the damage in the 1-direction due to a load in the 1-direction. Note that damage is only assumed to initiate once plastic strains have started to accumulate. Alternatively, if the damaged specimen was reloaded elastically in the 2-direction, due to the assumed damage coupling resulting from the load in the 1-direction, the reloaded specimen would have a reduced modulus in the 2-direction of E_{22}^{d11}. The reduced modulus is also a function of the damage induced by the load and resulting nonlinear deformation in the 1-direction as follows:

$$E_{22}^{d11} = \left(1 - d_{11}^{22}\left(\varepsilon_{11}^{p}\right)\right)E_{22} \tag{10}$$

where d_{11}^{22} is the damage in the 2-direction due to a load in the 1-direction. Similar arguments can be made and equations developed for the situation where the original specimen is loaded in the 2-direction.

For the case of multiaxial loading, the semicoupled formulation needs to account for the fact that as the load is applied in a particular coordinate direction, the loads are acting on damaged areas due to the loads in the other coordinate directions, and the load in a particular direction is just adding to the damaged area. For example, if one loaded the material in the 2-direction first, the reduced modulus in the 1-direction would be equal to E_{11}^{d22}. If one would then subsequently load the material in the 1-direction, the baseline modulus in the 1-direction would not be equal to the original modulus E_{11}, but instead the reduced modulus E_{11}^{d22}. Therefore, the loading in the 1-direction would result in the following further reduction in the modulus and effective area (A_{ij}) in the 1-direction:

$$\begin{aligned} E_{11}^{d11} &= \left(1 - d_{11}^{11}\left(\varepsilon_{11}^{p}\right)\right)E_{11}^{d22} = \left(1 - d_{11}^{11}\left(\varepsilon_{11}^{p}\right)\right)\left(1 - d_{22}^{11}\left(\varepsilon_{22}^{p}\right)\right)E_{11} \\ A_{11}^{d11} &= \left(1 - d_{11}^{11}\left(\varepsilon_{11}^{p}\right)\right)A_{11}^{d22} = \left(1 - d_{11}^{11}\left(\varepsilon_{11}^{p}\right)\right)\left(1 - d_{22}^{11}\left(\varepsilon_{22}^{p}\right)\right)A_{11} \end{aligned} \tag{11}$$

These results suggest that the relation between the actual stress and the effective stress should be based on a multiplicative combination of the damage terms as opposed to an additive combination of the damage terms. For example, for the case of plane stress, the relation between the actual and effective stresses could be expressed as follows:

$$\begin{aligned}
\sigma_{11} &= \left(1-d_{11}^{11}\right)\left(1-d_{22}^{11}\right)\left(1-d_{12}^{11}\right)\sigma_{11}^{\text{eff}} \\
\sigma_{22} &= \left(1-d_{11}^{22}\right)\left(1-d_{22}^{22}\right)\left(1-d_{12}^{22}\right)\sigma_{22}^{\text{eff}} \\
\sigma_{12} &= \left(1-d_{11}^{12}\right)\left(1-d_{22}^{12}\right)\left(1-d_{12}^{12}\right)\sigma_{12}^{\text{eff}}
\end{aligned} \tag{12}$$

where for each of the damage terms the subscript indicates the direction of the load which initiates the particular increment of damage and the superscript indicates the direction in which the damage takes place. For the full three-dimensional case the actual stresses would be functions of damage parameters in all six coordinate directions.

To properly characterize the damage model, an extensive set of test data is required. Due to the tabulated nature of the input, each of the damage parameters (d_{11}^{22} , d_{11}^{22} , etc.) has to be determined as a function of the plastic strain in a particular coordinate direction (such as ε_{11}^{p}). For example, to determine the damage terms for the case of loading in the 1-direction, a composite specimen has to be loaded to a certain plastic strain level in the 1-direction. The material is then unloaded to a state of zero stress, and then reloaded elastically in each of the coordinate directions to determine the reduced modulus of the material in each of the coordinate directions. Expressions such as those in Equations (9) and (10) can then be used to determine the required damage parameters for the particular value of plastic strain. The process needs to be repeated for multiple values of plastic strain in the 1-direction in order to establish the full characterization of the variation of the damage parameters as a function of the plastic strain in the 1-direction.

Failure Model

As discussed earlier in this paper, the majority of the available failure models utilize mathematical functions to describe the failure surface, which impose a specific shape on the failure surface. An example of this concept can be seen in Figure 1. In this figure, a two-dimensional failure surface in the σ_{11}-σ_{22} plane for the case of zero shear stresses generated using the Tsai-Wu failure model for a representative AS4/3501-6 polymer matrix composite is shown. The properties used to generate the failure surface were taken from Daniel and Ishai (Ref. 6) and are listed in Table 1. The two-dimensional version of the Tsai-Wu failure model that was used to generate the failure surface is as follows:

$$f_1\sigma_{11} + f_2\sigma_{22} + f_{11}\sigma_{11}^2 + f_{22}\sigma_{22}^2 + f_{66}\sigma_{12}^2 + 2f_{12}\sigma_{11}\sigma_{22} = 1 \tag{13}$$

where σ_{ij} are the stresses and the coefficients f_i and f_{ij} are defined as follows:

$$\begin{aligned}
f_1 &= \frac{1}{X_T} - \frac{1}{X_C} \qquad f_{11} = \frac{1}{X_T X_C} \qquad f_{66} = \frac{1}{S^2} \\
f_2 &= \frac{1}{Y_T} - \frac{1}{Y_C} \qquad f_{22} = \frac{1}{Y_T Y_C} \qquad f_{12} = -\frac{1}{2}\sqrt{f_{11} f_{22}}
\end{aligned} \tag{14}$$

where X_T is the longitudinal tensile failure stress, X_C is the longitudinal compressive failure stress, Y_T is the transverse tensile failure stress, Y_C is the transverse compressive failure stress and S is the in-plane shear failure stress. Note that the actual failure surface is continuous but slight discontinuities are shown in the presented graphs due to numerical issues in the generation of the graph. As can be seen in the

figure, the failure surface is elliptical due to the quadratic nature of the equation defining the failure surface. In reality, however, as shown for example in some of the cases discussed by Daniel and Ishai (Ref. 6), the failure surfaces of actual composites often do not exhibit this simple shape. A schematic of this idea is shown in Figure 2, where a representative example of a failure surface of a composite in the σ_{22}-σ_{12} plane is shown. This example failure surface cannot be easily defined by a mathematical function of the stresses. Alternatively, as shown in the figure, one potential method of defining the points in the failure surface is to use a cylindrical type of coordinate system. In this approach, a variable θ defines the relative location of the point on the failure surface in stress space, while a second variable r defines the "magnitude" of the failure surface point in the stress space location. Since the relationship between "r" and "θ" also cannot be easily defined by a mathematical function for a realistic composite failure surface, a tabulated approach, where a series of "r" and "θ" pairs are explicitly defined for a given failure surface, can provide a more accurate representation of the failure surface. Buyak (Ref. 19) has demonstrated that tabulated approaches can be successful in defining complex failure surfaces for advanced materials based on experimental data. The tabulated approach allows for the use of experimentally defined failure surface data, a failure surface defined using any existing failure model, or a combination of experimental and numerically obtained "virtual" data. The combined approach can allow for the case where actual failure data is only available for a portion of the total stress space, with "virtual" data being required to fill in the gaps in the failure surface.

Independent and Dependent Variables

As described above, for the tabulated failure surface definition proposed in this study appropriate independent and dependent variables need to be defined. The independent variables need to define the location of a point on the failure surface in stress space, and the dependent variable needs to define the magnitude of the failure surface point along the lines defined by the independent variables. For the current approach, the in-plane and out-of-plane responses will be considered separately. First, the definition of the in-plane failure surface will be discussed. For the in-plane failure surface definition, two independent variables are defined. The first independent variable will be the ratio of the shear stress to the shear failure stress. For selected values of this shear ratio, the location of each defined point on the failure surface in stress space is specified by defining the angle of the point in the σ_{11}-σ_{22} plane, which becomes the second independent variable. This concept is illustrated in Figure 1 using the Tsai-Wu failure surface (for the case of zero shear stress) discussed earlier. Using simple geometric principals, the angle θ for each defined point on the failure surface can be defined in terms of the stresses σ_{11} and σ_{22} as shown below. To ensure a set of unique, monotonically increasing angles from –180° to 180°, if the stress σ_{22} is negative the computed angle is multiplied by –1 as shown below:

$$\theta = \cos^{-1}\left(\frac{\sigma_{11}}{\sqrt{\sigma_{11}^2 + \sigma_{22}^2}}\right) \qquad (15)$$

$$\theta_{act} = -\theta \text{ if } \sigma_{22} \le 0$$

For the dependent variable, which is used to define the magnitude of the failure surface point given a particular location in stress space, a stress invariant first identified by Fleischer (Ref. 20) is used, defined as follows for the plane stress case:

$$r = \sqrt{\sigma_{11}^2 + \sigma_{22}^2 + 2\sigma_{12}^2} \qquad (16)$$

This invariant can be considered to be like a "radius" from the origin to the failure surface. The factor of 2 in front of the shear stress term reflects the symmetry of the stress tensor. Stresses or strains can be used

in defining the dependent variable, making the model more general. Using an invariant type of term also allows for the stress interactions to be more appropriately accounted for in the failure definition and helps to ensure that the failure definition will be accurate for a variety of loading conditions. The general concept of the "radius" of the failure surface is shown in Figure 1.

One difficulty in using a tabulated approach of this type is that for many polymer matrix composites the failure surface is highly anisotropic due to the high failure strength in the fiber direction and the much lower failure stresses in the transverse direction. This anisotropy can be observed graphically in Figure 3, in which a version of the failure surface shown in Figure 1 is shown. In this plot, the range of the y axis is adjusted to be equal to the range of the x axis. As can be seen in this figure, the actual failure surface is highly elongated. The consequences of the significant elongation of the failure surface can be observed in Figure 4, where the radius versus the angle is plotted for the failure surface defined above. As can be seen in the figure, the majority of the points of the failure surface are clustered at angles near –180°, 0°, and 180°. This clustering would create round-off and interpolation difficulties in the numerical implementation of the failure model, making the current definition undesirable.

To facilitate a more even distribution of the tabulated failure surface points along the entire spectrum of angles, the stresses used in the definition of the independent variable θ can be scaled. For the current method, the stresses in the 11-direction are arbitrarily scaled by the longitudinal tensile failure stress, and the 22-direction stresses are scaled by the transverse tensile failure stress. Revised angles are then computed using these scaled stresses as shown below. The value of the dependent variable r, however, is still computed using the actual unscaled stresses:

$$\begin{aligned}
\sigma_{11-\text{scaled}} &= \frac{\sigma_{11}}{X_T} \\
\sigma_{22-\text{scaled}} &= \frac{\sigma_{22}}{Y_T} \\
\theta &= \cos^{-1}\left(\frac{\sigma_{11-\text{scaled}}}{\sqrt{\sigma_{11-\text{scaled}}^2 + \sigma_{22-\text{scaled}}^2}} \right) \\
\theta_{\text{act}} &= -\theta \text{ if } \sigma_{22} \le 0
\end{aligned} \tag{17}$$

The modified version of the failure surface defined in Figure 1 is shown in Figure 5. The overall shape of the failure surface is identical, only the relative values of the axes have changed. A revised plot of the radius versus the scaled angle is shown in Figure 6. As can be seen in this figure as compared to Figure 4, the points defining the failure surface are much more evenly distributed along the range of angles and the sharp points observed in the graph in Figure 4 are smoothed out. This relationship, particularly when transferred to a tabulated format, will allow for much smoother and more accurate interpolations when used in a numerical implementation.

As mentioned earlier, for the proposed approach the procedure described above needs to be repeated for several ratios of the shear stress to the shear failure stress in order to fully define the in-plane failure surface. An example of the scaled failure surface in the σ_{11}-σ_{22} plane where the shear stress is equal to 50 percent of the shear failure stress is shown in Figure 7. In this plot, the failure surface for the case with zero shear stresses is shown in green for comparison. In this plot, one can observe that increasing the shear stresses results in a failure surface with the same shape as the surface generated assuming zero shear stresses, but the location of the failure surface is shifted somewhat towards the negative stress quadrant of the graph. A plot of the radius versus the scaled angle for the 50 percent shear case is shown in Figure 8, along with the plot for the zero shear stress case for comparison (shown in green). Comparing the two plots, the relative shapes of the two curves are similar, but the magnitudes of the radius values for the 50 percent shear stress case are somewhat lower.

Modified Center of Failure Surface

As can be observed in Figure 7, the failure surfaces are not centered at the origin, and as the shear stress is increased the failure surface becomes even more skewed away from the origin. At high values of shear stresses, the failure surface may not even include the origin. Even when the origin is included, the fact that the failure surface is not centered on the origin may cause the angle calculations to be skewed. If the failure surface does not include the origin, the angle calculations would not even be valid as they would not be unique.

To mitigate this issue, in the current approach the origin of the scaled failure surfaces for the selected shear stress ratios is redefined such that it lies in the center of the failure surface. The modified center of the failure surface is defined based on the maximum and minimum scaled stress values in the 11- and 22-directions as shown below. Modified stresses in the 11- and 22-directions are then defined in terms of the modified center as shown below:

$$\begin{aligned}
\sigma_{11-\text{center}} &= \frac{1}{2}\left(\sigma_{11-\max} + \sigma_{11-\min}\right) \\
\sigma_{22-\text{center}} &= \frac{1}{2}\left(\sigma_{22-\max} + \sigma_{22-\min}\right) \\
\sigma_{11-\text{mod}} &= \sigma_{11-\text{scaled}} - \sigma_{11-\text{center}} \\
\sigma_{22-\text{mod}} &= \sigma_{22-\text{scaled}} - \sigma_{22-\text{center}}
\end{aligned} \tag{18}$$

The angle calculations shown in Equations (15) and (17) are carried out using the revised stresses. The radius calculations are carried out using the original, unscaled and unmodified stresses. The modified, scaled, re-centered failure surfaces are shown in Figure 9, where the modified surface for the case of zero shear stress is shown in green and the modified failure surface for the case where the shear stresses are equal to 50 percent of the shear failure stress is shown in black. In both cases, the overall shape of the failure surface does not change from the original case but the failure surfaces are now centered about the modified origin.

The radius versus scaled angle plots for the zero shear case (green curve) and for the 50 percent shear ratio case (black curve) determined using the modified failure surface centers are shown in Figure 10. In both cases, the tabulated points defining the failure surface are more evenly distributed compared to the cases with the original origin location. This improvement in the failure point distribution will improve the implementation of the failure model.

Algorithm for Implementation of In-Plane Failure Model

To apply the in-plane version of the failure model described above, first the failure surface for a given composite needs to be converted into a tabulated form in order to establish a benchmark for determination if failure has occurred for a given load condition. The baseline failure surface for a given material can be established based on experimental data, any available numerical failure model, or a combination of the two. In the combination approach, experimental data can be used where available, and analytically generated data can be used to fill in the required gaps. Given the baseline failure surface data, Equations (15) to (18) are then used to generate a series of "radius" versus "angle" plots for various ratios of shear stress to shear failure stress, similar to Figures 13 and 14. For use in a numerical algorithm, the data needs to be transformed into a set of tables which serve as input to the computer model. The stress values defining the "center" of the failure surface for the selected shear stress ratios also need to be defined for use in the calculations.

The specific algorithm to implement the failure model is as follows:

1. Given: applied load condition σ_{11}, σ_{22}, σ_{12}
2. Compute the shear ratio $R = \sigma_{12}/S$
3. Scale the longitudinal and transverse stresses:

$$\sigma_{11-\text{scaled}} = \frac{\sigma_{11}}{X_T}$$
$$\sigma_{22-\text{scaled}} = \frac{\sigma_{22}}{Y_T} \tag{19}$$

4. Look up the appropriate modified failure surface center stresses ($\sigma_{11\text{-center}}$ and $\sigma_{22\text{-center}}$) (Eq. (18)) corresponding to the current shear ratio R. Note that interpolation of these stresses may be required if the current shear ratio R is not explicitly defined in the input tables.
5. Compute the modified longitudinal and transverse stresses given the stresses defining the modified failure surface center:

$$\sigma_{11-\text{mod}} = \sigma_{11-\text{scaled}} - \sigma_{11-\text{center}}$$
$$\sigma_{22-\text{mod}} = \sigma_{22-\text{scaled}} - \sigma_{22-\text{center}} \tag{20}$$

6. Compute the angle θ associated with the modified longitudinal and transverse stresses:

$$\theta = \cos^{-1}\left(\frac{\sigma_{11-\text{mod}}}{\sqrt{\sigma_{11-\text{mod}}^2 + \sigma_{22-\text{mod}}^2}}\right)$$
$$\theta_{\text{act}} = -\theta \; \textit{if} \; \sigma_{22-\text{mod}} \le 0 \tag{21}$$

7. Compute the radius associated with the unscaled, unmodified applied stresses:

$$r = \sqrt{\sigma_{11}^2 + \sigma_{22}^2 + 2\sigma_{12}^2} \tag{22}$$

8. Compare the radius computed at step 7 to the tabulated radius at failure for the given shear ratio R and angle θ. Note that interpolation of the radius at failure may be required if the specific values of R and θ are not specified in the input tables.
9. If the radius computed using the applied stresses is equal to or greater than the radius at failure, the material is assumed to have failed. In the numerical implementation, the element will either be eroded once failure is deemed to have occurred or have all of its stiffness properties reduced to negligible values. A progressive reduction in stresses will not occur.

Out-of-Plane Failure Surface Definition and Modification of Failure Model

The methodology and procedures described above are valid for the case of in-plane loading and stresses. For thin composites, particularly under in-plane loading, this case is most likely sufficient since the out-of-plane normal and transverse shear stresses can be assumed to be negligible. However, for thicker composites, particularly under impact loading conditions, the out-of-plane stresses can often be significant and must be included. One way to account for failure due to out-of-plane stresses is to utilize a delamination model, as is discussed in many sources such as Barbero (Ref. 17). In this case, the in-plane

failure model could be used in combination with a delamination model to fully define the composite failure. However, an alternative approach would be to define a tabulated failure surface specified by the out-of-plane stresses that is independent from the failure surface defined by the in-plane stresses. As will be described below, the out-of-plane failure surface can be defined in a manner similar to what was used to define the in-plane failure surface. The radius-like dependent variable can then be used to couple the failure responses due to the in-plane and out-of-plane stresses.

To generate the required out-of-plane failure surfaces, a series of two-dimensional failure surfaces in the σ_{13}-σ_{23} plane are defined for various ratios of the out-of-plane normal stress σ_{33} to the out-of-plane normal failure stress. Equations similar to Equations (15), (17), and (18) can then be used to define the values of the angle θ (where σ_{11} in the equations is replaced with σ_{13} and σ_{22} in the equations is replaced with σ_{23}) for the out-of-plane failure surfaces. For the dependent variable, a stress invariant radius term similar to Equation (16) is defined:

$$r = \sqrt{\sigma_{33}^2 + 2\sigma_{13}^2 + 2\sigma_{23}^2} \tag{23}$$

where the transverse shear stresses are multiplied by two due to the symmetry of the stress tensor. Plots of the radius versus scaled angle (similar to those shown in Fig. 10) can then be generated for several out-of-plane normal stress ratios based on the out-of-plane failure stresses and converted into a tabulated set of input for the failure model. For a given out-of-plane loading condition, the out-of-plane normal stress to out-of-plane normal failure stress ratio, angle and radius can be computed using a process similar to the process used for the in-plane stresses. The radius computed using the current stresses can then be compared to the corresponding radius at failure to determine if failure has occurred.

For the case where both in-plane and out-of-plane stresses are present in a material under a specified load state, a method needs to be specified to allow for the stress interactions that may take place under the combination of in-plane and out-of-plane loading. Accounting for the interaction is important because the combination of stresses may cause failure in the material even though the individual in-plane and out-of-plane criteria may not indicate that failure has occurred. To account for the stress interaction, a ratio d_{ip} and a ratio d_{oop} are defined. The ratio d_{ip} represents the ratio of the radius computed using Equation (16) for the applied in-plane stresses to the corresponding radius computed using the in-plane stresses at failure for a given angle and shear stress ratio. The ratio d_{oop} represents the ratio of the radius computed using Equation (23) for the applied out-of-plane stresses to the radius at failure for a given out-of-plane angle and out-of-plane normal stress ratio. A weighted sum of the ratios can then be computed using the following expression, where n is an arbitrary number defined by the user:

$$d = \sqrt[n]{d_{ip}^n + d_{oop}^n} \tag{24}$$

If the weighted ratio d is greater than or equal to one, failure is assumed to have occurred. If the weighted ratio d is less than one, failure is assumed to have not occurred.

Conclusions

A generalized composite model suitable for use in polymer composite impact simulations has been developed. The model utilizes a plasticity based deformation model obtained by generalizing the Tsai-Wu failure criteria. A strain equivalent damage model has also been developed in which loading the material in a particular loading direction can lead to damage in multiple coordinate directions. A general, tabulated failure model has also been formulated. Within the failure model, a methodology has been developed to convert two-dimensional failure surfaces to a tabulated format based on the location of the points of the failure surface in stress space and a dependent stress invariant variable which defines the magnitude of the

failure stress points at a given location. An algorithm to implement the failure model has been developed, and a procedure for accounting for a combination of in-plane and out-of-plane stresses has been specified.

Future efforts will include developing the detailed numerical algorithms required to implement the damage and failure models into the material model being developed for inclusion within the LS-DYNA computer code. The failure model will also be refined to include appropriate techniques for element removal once the failure criteria has been satisfied. Methods to account for delamination failure will also be formulated. Extensive sets of verification and validation studies will also be undertaken in order to fully exercise the developed model.

References

1. Hallquist, J. 2013. *LS-DYNA Keyword User's Manual*, *Version 970*. Livermore Software Technology Corporation, Livermore, CA.
2. Sun, C.T., and J.L. Chen. 1989. "A Simple Flow Rule for Characterizing Nonlinear Behavior of Fiber Composites," Journal of Composite Materials, 23:1009-1020.
3. Matzenmiller, A., J. Lubliner, and R.L. Taylor. 1995. "A constitutive model for anisotropic damage in fiber-composites," Mechanics of Materials, 20:125-152.
4. Goldberg, R., K. Carney, P. DuBois, C. Hoffarth, J. Harrington, S. Rajan, and G. Blankenhorn. 2014. "Theoretical Development of an Orthotropic Elasto-Plastic Generalized Composite Model," NASA/TM—2014-218347, National Aeronautics and Space Administration, Washington, D.C.
5. Goldberg, R., K. Carney, P. DuBois, C. Hoffarth, S. Rajan, and G. Blankenhorn. 2015. "Incorporation of Plasticity and Damage Into an Orthrotropic Three-Dimensional Model With Tabulated Input Suitable for Use in Composite Impact Problems," NASA/TM—2015-218849, National Aeronautics and Space Administration, Washington, D.C.
6. Daniel, I.M., and O. Ishai. 2006. *Engineering Mechanics of Composite Materials Second Edition*. Oxford University Press, New York.
7. Hashin, Z. 1980. "Failure Criteria for Unidirectional Fiber Composites," Journal of Applied Mechanics, 47:329-334.
8. Puck, A., and H. Schurmann. 1998. "Failure Analysis of FRP Laminates by Means of Physically Based Phenomenological Models," Composites Science and Technology, 58:1045–1067.
9. Pinho, S.T., L. Iannucci, and P. Robinson. 2006. "Physically-Based Failure Models and Criteria for Laminated Fibre-Reinforced Composites With Emphasis on Fibre Kinking: Part I: Development," Composites: Part A, 37:63-73.
10. Maimi, P., P.P. Camanho, J.A. Mayugo, and C.G. Davila. 2007. "A Continuum Damage Model for Composite Laminates: Part I-Constitutive Model," Mechanics of Materials, 39:897-908.
11. Mayes, J.S., and A.C. Hansen. 2001. "Multicontinuum Failure Analysis of Composite Structural Laminates," Mechanics of Composite Materials and Structures, 8:249-262.
12. Feng, W.W. 1991. "A Failure Criterion for Composite Materials," Journal of Composite Materials, 25:88-100.
13. Hinton, M.J., and A.S. Kaddour. 2012. "The background to the Second World-Wide Failure Exercise," Journal of Composite Materials, 46:2283-2294.
14. Kaddour, A.S., M.J. Hinton, P.A. Smith and S. Lee. 2013. "The background to the third world-wide failure exercise," Journal of Composite Materials, 47:2417-2426.
15. Kaddour, A.S., M.J. Hinton, P.A. Smith and S. Lee. 2013. "A comparison between the predictive capability of matrix cracking, damage and failure criteria for fibre reinforced composite laminates: Part A of the third world-wide failure exercise," Journal of Composite Materias, 47:2749-2779.
16. Khan, A.S., and S. Huang. 1995. Continuum Theory of Plasticity. John Wiley and Sons, New York.
17. Barbero, E.J. 2013. Finite Element Analysis of Composite Materials Using ABAQUS. CRC Press, Boca Raton, FL.
18. Lemaitre, J., and R. Desmorat. 2005. Engineering Damage Mechanics: Ductile, Creep and Brittle Failures. Springer, Berlin.

19. Buyak, M. 2014. “Development of a New Metal Material Model in LS-DYNA Part 2: Development of A Tabulated Thermo-Viscoplastic Material Model With Regularized Failure for Dynamic Ductile Failure Prediction of Structures Under Impact Loading,” DOT/FAA/TC-13/25, P2, Federal Aviation Administration, Washington, D.C.
20. Fleischer M., T. Borrvall, and K.-U. Bletzinger. 2007. “Experience from using recently implemented enhancements for Material 36 in LS-DYNA 971 performing a virtual tensile test,” 6th European LS-DYNA Users Conference, Gothenburg, Sweden.

TABLE 1.—MATERIAL PROPERTIES FOR AS4/3501-6 UNIDIRECTIONAL COMPOSITE

Property	Value
Longitudinal Modulus E_{11} (GPa)	147
Transverse Modulus E_{22} (GPa)	10.3
Longitudinal Poisson’s Ratio ν_{12}	0.27
Transverse Poisson’s Ratio ν_{23}	0.54
In-Plane Shear Modulus G_{12} (GPa)	7.0
Longitudinal Tensile Strength X_T (MPa)	2280
Longitudinal Compressive Strength X_C (MPa)	1725
Transverse Tensile Strength Y_T (MPa)	57
Transverse Compressive Strength Y_C (MPa)	228
In-Plane Shear Strength S (MPa)	76

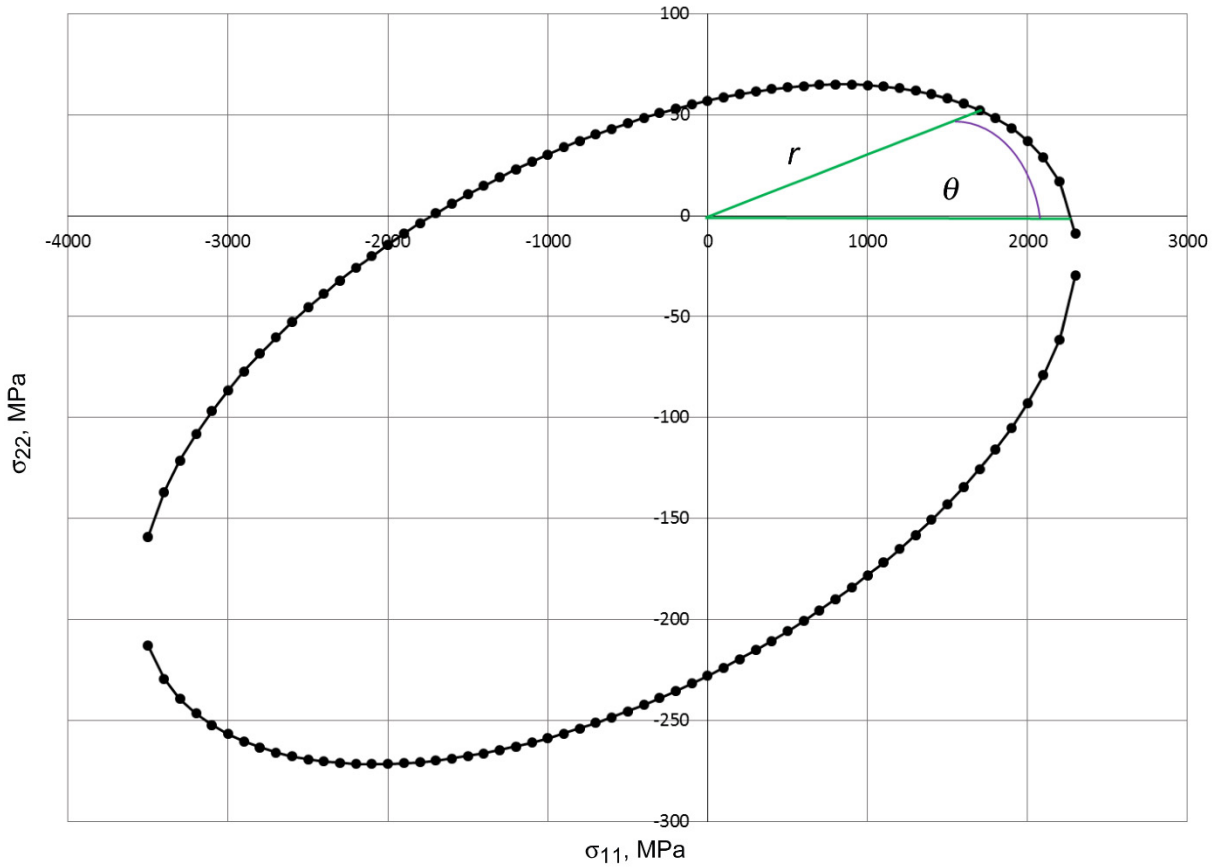

Figure 1.—Tsai-Wu failure surface for AS4/3501-6 composite. Variables θ and r used to specify tabulated failure surface are also defined.

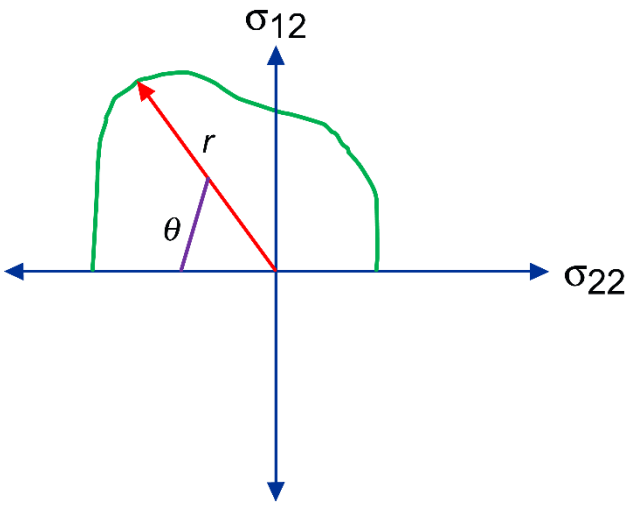

Figure 2.—Schematic of failure surface for representative composite.

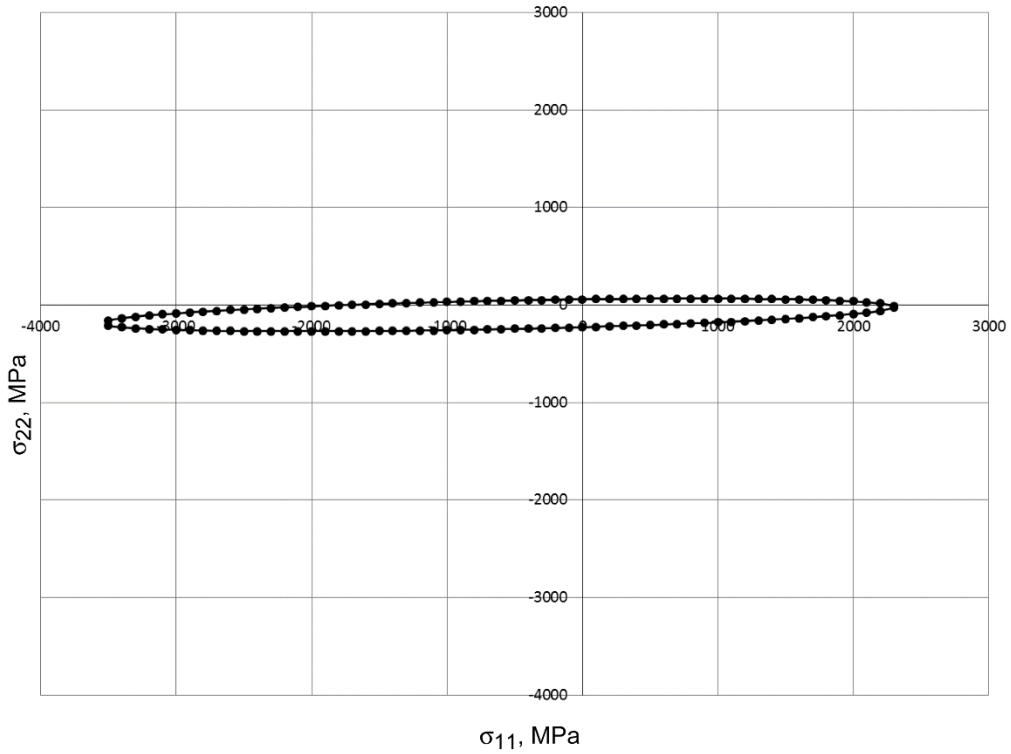

Figure 3.—Tsai-Wu surface for AS4/3501-6 composite with equal x and y axis ranges.

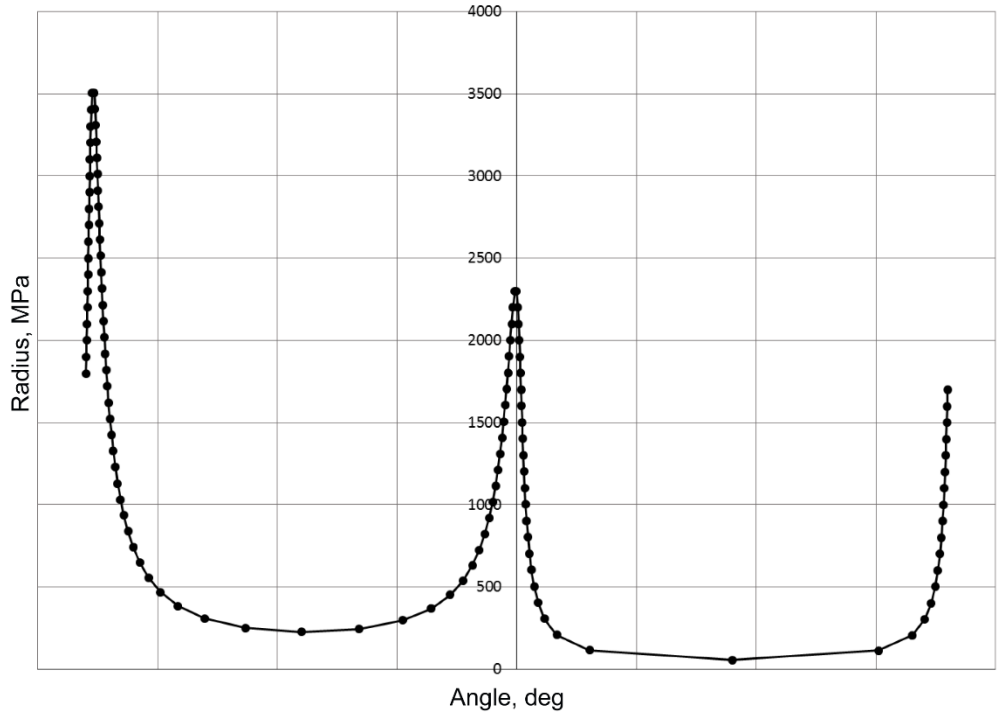

Figure 4.—Plot of radius vs. angle for original AS4/3501-6 failure surface.

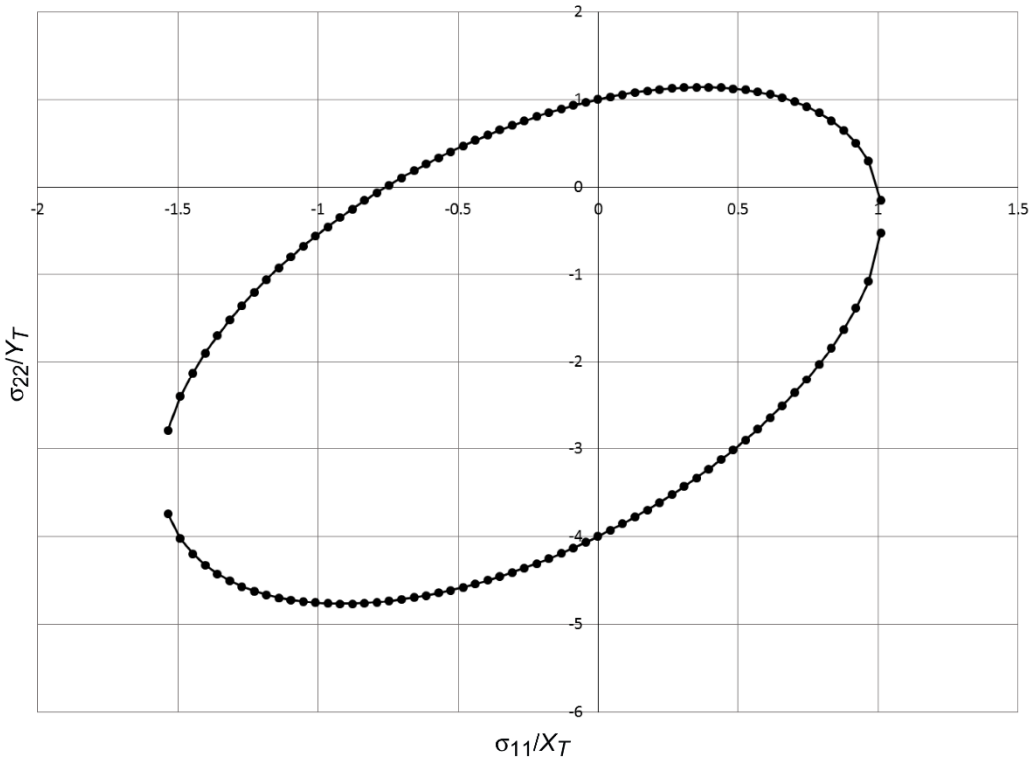

Figure 5.—Scaled Tsai-Wu failure surface for AS4/3501-6 composite.

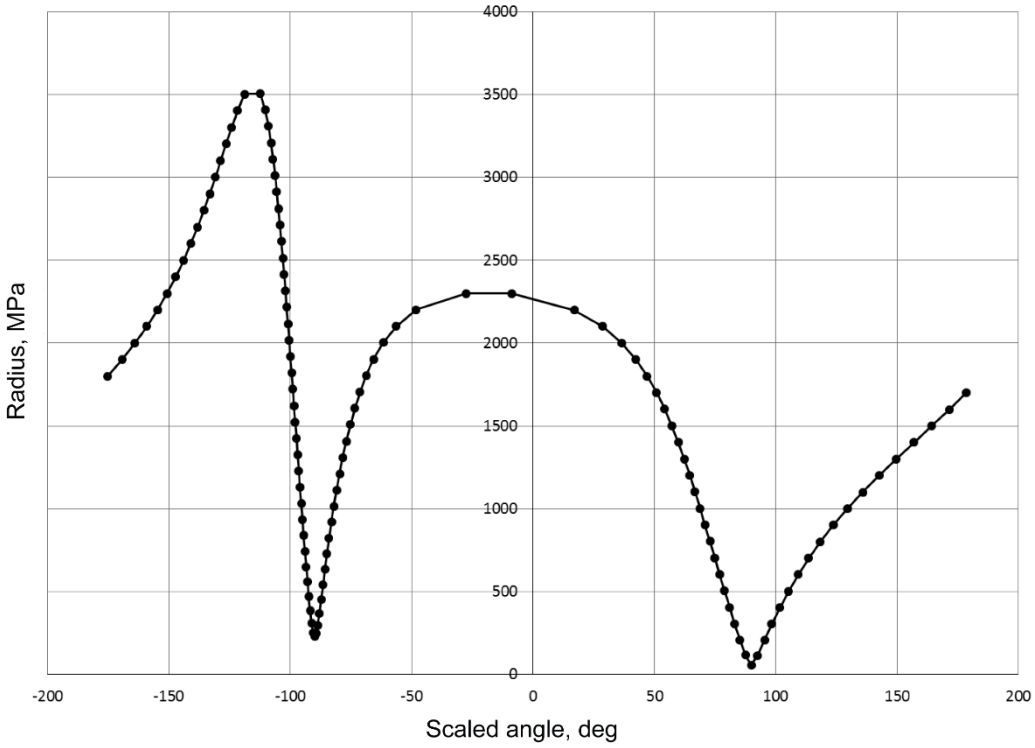

Figure 6.—Plot of radius versus angle for scaled AS4/3501-6 failure surface.

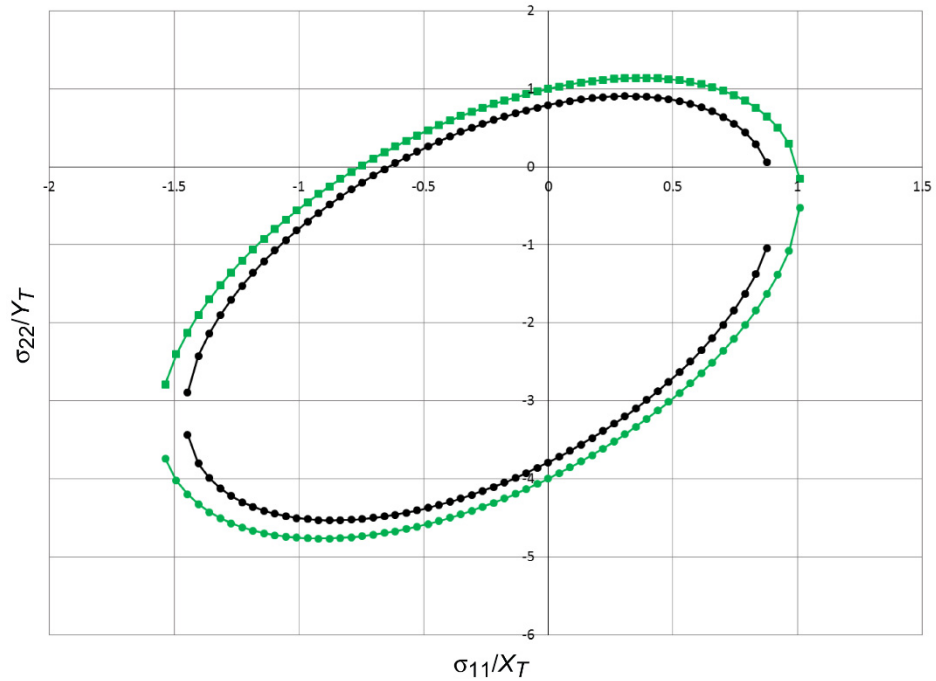

Figure 7.—Scaled Tsai-Wu failure surface with shear stress equal to 50 percent of shear failure stress for AS4/3501-6 composite (black curve). Failure surface with zero shear stress shown in green.

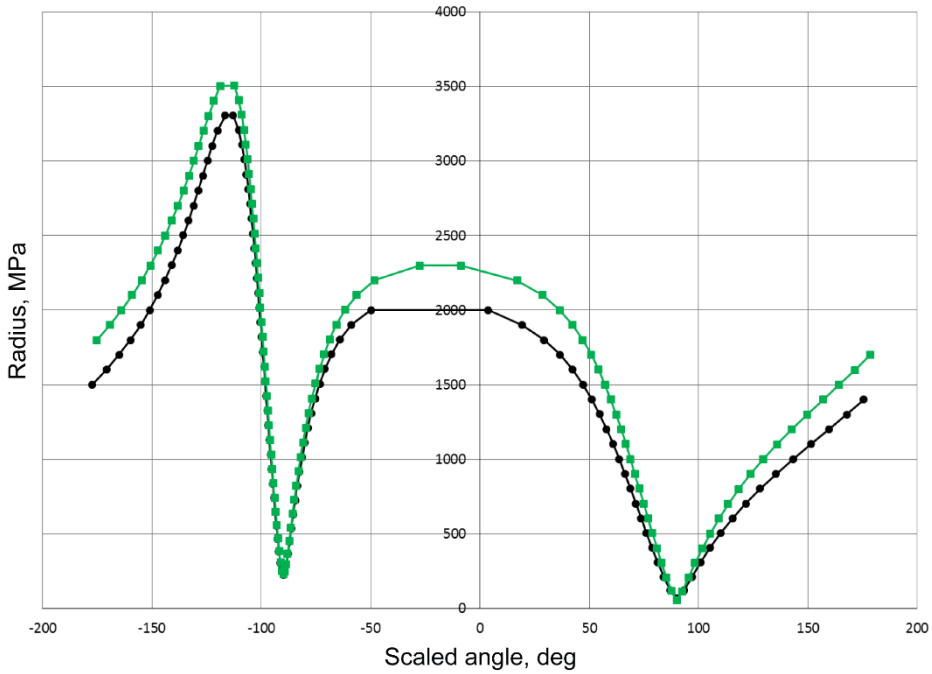

Figure 8.—Plot of radius versus angle for scaled AS4/3501-6 failure surface for case with shear stress equal to 50 percent of shear failure stress (black curve) and for case of zero shear stress (green curve).

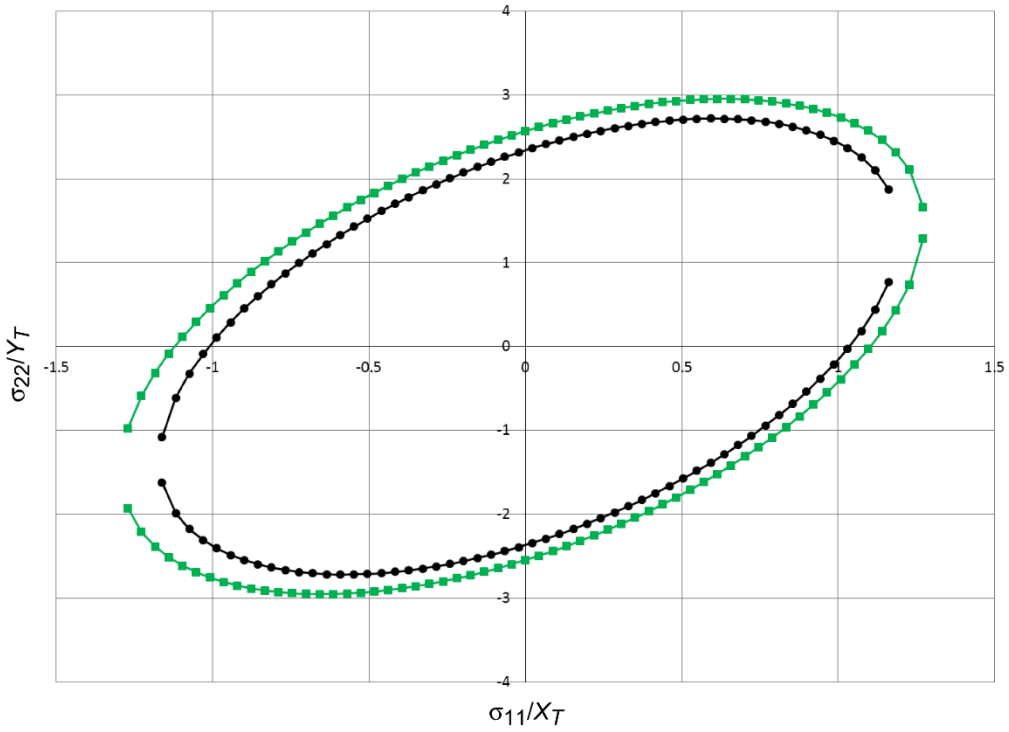

Figure 9.—Scaled Tsai-Wu failure surface with modified center for AS4/3501-6 composite. Surface for case with zero shear stress shown in green, surface for case with shear stress equal to 50 percent of shear failure stress shown in black.

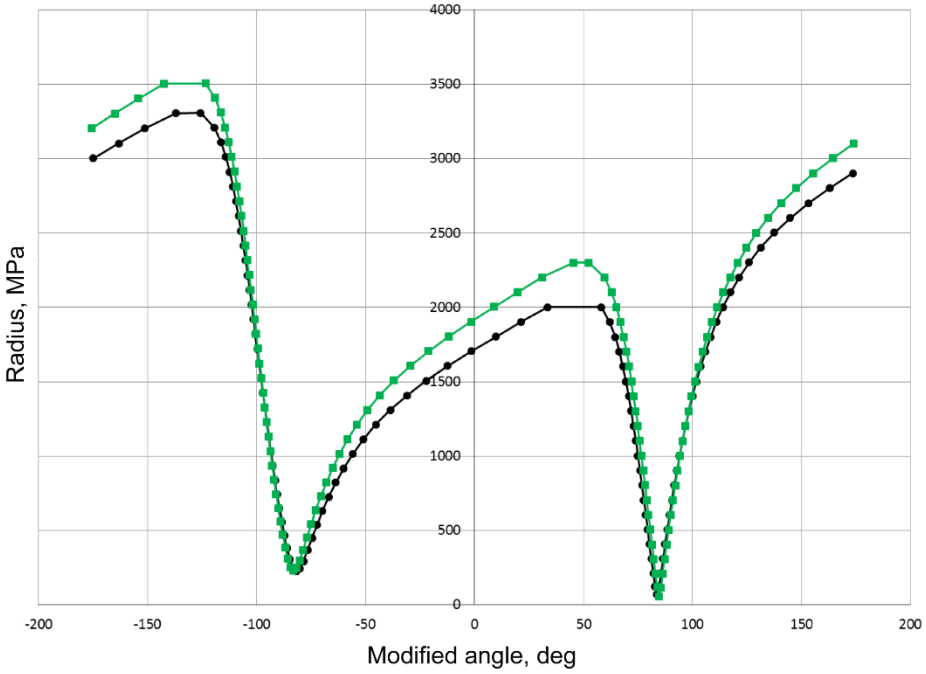

Figure 10.—Plot of radius versus angle for scaled failure surface with modified center for AS4/3501-6 composite for case of zero shear stresses (green curve) and case where shear stresses equal 50 percent of shear failure stress (black curve).